Applied Catalysis B: Environmental 127 (2012) 112–120

Contents lists available at SciVerse ScienceDirect

Applied Catalysis B: Environmental

journal homepage: www.elsevier.com/locate/apcatb

Effect of deposition of silver on structural characteristics and photoactivity of TiO_2-based photocatalysts

E. Pulido Melián[a,*], O. González Díaz[a,*], J.M. Doña Rodríguez[a], G. Colón[b], J.A. Navío[b], M. Macías[b], J. Pérez Peña[a]

[a] Centro Instrumental Físicoquímico para el desarrollo de Investigación Aplicada (CIDIA-FEAM), Departamento de Química, Universidad de Las Palmas de Gran Canaria, Edificio Polivalente I del Parque Científico Tecnológico, Campus de Tafira, 35017 Las Palmas de Gran Canaria, Spain
[b] Instituto de Ciencia de Materiales de Sevilla, Centro Mixto CSIC-Universidad de Sevilla, 41092 Américo Vespucio s/n, Sevilla, Spain

ARTICLE INFO

Article history:
Received 22 March 2012
Received in revised form 18 July 2012
Accepted 9 August 2012
Available online 17 August 2012

Keywords:
TiO_2
Silver
Impregnation
Photodeposition
Photocatalysis
Phenol

ABSTRACT

The homemade bare TiO_2 photocatalyst obtained in a previous work was modified with nanosized silver particles by liquid impregnation and photodeposition methods to obtain different noble metal loadings (0.3–1 at.%). Characterization of the synthesized photocatalysts was carried out by the BET method, XPS, TEM, SEM-EDX, XRD and diffuse reflectance measurements. Photocatalytic activity of these silver-deposited TiO_2 nanoparticles was tested by photocatalytic degradation of phenol as a reference model representing phenolic pollutants. The noble metal content on the TiO_2 surface affected the efficiency of the photocatalytic process, and the photocatalytic activity of noble metal-modified TiO_2 was considerably better than that of bare TiO_2. Phenol decomposition rate was higher with TiO_2 modified by the liquid impregnation method than with TiO_2 modified by the photodeposition method.

1. Introduction

TiO_2 heterogeneous photocatalysis has recently been the subject of numerous investigations as it is an attractive technique for the complete destruction of undesirable contaminants both in aqueous and in gas phase [1,2] by using solar or artificial light illumination. Upon band-gap excitation of TiO_2, the photoinduced electrons and positively charged holes can respectively reduce and oxidize species adsorbed on the semiconductor particles. The high degree of recombination between photogenerated electrons and holes is a major rate-limiting factor controlling photocatalytic efficiency. Enhancement of TiO_2 photocatalytic activity is one of the most important aspects of heterogeneous photocatalysis [3]. Modification of photocatalysts with noble metals such as Pt, Au and Pd, is a procedure used to obtain more efficient photocatalysts [4–6]. Most research involving photocatalysis with noble metals is focused on the transference of electrons photoinduced by UV radiation from the conduction band of TiO_2 to the metal deposits. The positive effects of the noble metal deposits on photocatalytic activity are several [7–10]: (i) improvement of the electron–hole separation by trapping the electrons speeding up the formation of $O_2^{\bullet -}$, (ii) shift of light absorption into the visible-light range due to plasmon formation, (iii) modification of the surface adsorption properties of the photocatalysts and (iv) generation of hydroxyl radicals through the reaction with hydrogen peroxide produced by oxygen photoreduction as:

$$M + H_2O_2(ads) + H^+(aq) \rightarrow HO^\bullet + H_2O + M^+$$

However, the amount of metal cannot be increased indefinitely. Negative effects of the presence of metal deposits on the photocatalyst surface have been described that lead to decreased photon efficiency. When metal concentration is high and, therefore, metal clusters numerous and large: (i) the negatively charged metal particles can act as recombination centers trapping holes [11], (ii) more semiconductor surface is covered by deposits decreasing the light that reaches its surface and, consequently, the number of photogenerated electron–hole pairs [12] and (iii) metal deposits can occupy the semiconductor surface active centers [13]. In the case of silver-deposited systems, the literature highlights an optimum percentage around 0.5–1.0 at.% Ag above which photoefficiency decreases.

Photocatalytic activity is not only dependent on metal type and the concentration and characteristics of the deposits, but also to a major extent on the TiO_2 base [14]. For this reason, apparently contradictory results can be found in the literature about the effects of

* Corresponding authors. Tel.: +34 928457298; fax: +34 928457397.
E-mail addresses: elisendapm80@hotmail.com (E. Pulido Melián), ogonzalez@dqui.ulpgc.es (O. González Díaz).

0926-3373/$ – see front matter © 2012 Elsevier B.V. All rights reserved.
http://dx.doi.org/10.1016/j.apcatb.2012.08.007

a particular metal, and there are no general rules as to whether one metal is better than another or what their optimum concentrations are. The establishment of rules in photocatalysis is even more complicated since the activity will also depend on the pollutant subject to degradation [15].

In recent years, the silver ion has caught the attention of a lot of researchers due to the increased photoactivity and bactericidal effect of photocatalysts which contain it. Kondo et al. [16] reported that Ag/TiO_2 was more effective than bare TiO_2 in chloroform degradation; Sahoo et al. [17] in the degradation of C.I. Basic Violet 3; Ozkan et al. [18] in the degradation of Sirius Gelb GC dye; and Behnajady et al. [19] in the degradation of Acid Red 88 dye.

The usual methods for surface modification of TiO_2 with noble metals are: thermal impregnation [20] and photodeposition [11]. There is some debate as to which method leads to more efficient photocatalysts due to the lack of studies that compare them under the same conditions. It was therefore decided to use both methods in this paper to study the effect of the surface deposition of Ag on the structure and photoactivity of a homemade TiO_2-based photocatalyst [21]. As reference, the commercially available Degussa P25 TiO_2 was subjected to the same study.

2. Experimental

2.1. Equipment and methods

BET surface area and porosity measurements were carried out by N_2 adsorption at 77 K using a Micromeritics ASAP 2010 instrument.

Phase composition and the degree of crystallinity in the samples were determined by X-ray diffraction (XRD). XRD patterns were recorded on a Siemens D-501 diffractometer equipped with a Ni filter and graphite monochromator using Cu Kα radiation ($\lambda = 1.5418$ Å). Crystal sizes in the different phases were estimated from line broadening of the corresponding X-ray diffraction peaks by using the Scherrer equation. Peaks were fitted using the Voigt function ($R^2 > 0.995$).

Light absorption properties of the samples were studied by UV–vis spectroscopy. UV–vis spectra were recorded on a Varian Cary 100 spectrometer equipped with an integrating sphere using $BaSO_4$ as reference. Both absorbance and diffuse reflectance spectra were recorded for all samples and the Kubelka–Munk function, $F(R_\infty)$, was applied to obtain a magnitude proportional to the extinction coefficient. Band-gaps were calculated by the Kubelka–Munk function, following the method proposed by Tandon and Gupta [22].

The morphology of the samples and the dispersion and size of surface metal deposits were studied by transmission electron microscopy (TEM) using a Philips CM 200 instrument and by scanning electron microscopy (SEM) using a Jeol JSM-5400 apparatus equipped with an X-ray dispersive energy (EDX) analyzer.

Surface characterization by X-ray photoelectron spectroscopy (XPS) was conducted on a Leybold–Heraeus LHS-10 spectrometer, working with constant pass energy of 50 eV. The spectrometer main chamber was maintained at a pressure $<2 \times 10^{-9}$ Torr, and the machine was equipped with an EA-200 MCD hemispherical electron analyzer with a dual X-ray source of Al Kα ($h\nu$) 1486.6 eV at 120 W and 30 mA. The carbon 1s signal (284.6 eV) was used as the internal energy reference in all the measurements. Samples were outgassed in the prechamber of the instrument at 150 °C up to a pressure $<2 \times 10^{-8}$ Torr to remove chemisorbed water from their surfaces.

The total concentration of dissolved Ag for recyclability runs was measured by means of atomic absorption spectrophotometry (AAS – Varian SpectrAA model), with Zeeman background correction and equipped with an electrothermal atomizer.

The photocatalytic activity of the samples was evaluated in the phenol photo-oxidation reaction. Suspensions of the samples in aqueous phenol solution (50 ppm) were placed in a Pyrex immersion well photoreactor (500 mL) and illuminated for 2 h by a HPK125 W Hg lamp supplied by Philips showing main emission line at 365 nm. The photonic flow per unit area of the incident UV light (200–400 nm) on the solution was determined to be approximately 1.4×10^{15} photons cm^{-2} s^{-1} using an Ocean Optics HR2000+ spectrometer. Magnetic stirring and a constant flow of oxygen maintained the homogeneous suspension of photocatalyst in the solution. Prior to illumination, photocatalyst–substrate equilibration was ensured by stirring the suspension for 30 min in the dark. The evolution of the phenol concentration was measured by HPLC using a Discovery C18 (25 cm × 4.6 mm, 5 μm) column and an acetonitrile–water–acetic acid (40:59.6:0.4% (v/v/v)) mobile phase, with a UV detector ($\lambda = 270$ nm). Total organic carbon (TOC) was measured using a Shimadzu TOC VCSN analyzer.

2.2. Catalyst preparation

TiO_2 (Degussa, P25) and a homemade photocatalyst obtained by sol-gel and hydrothermal synthesis (detailed characterization of the TiO_2ht600 sample has been reported in a previous paper [21]) were used as initial photocatalytic materials. Silver nitrate, $AgNO_3$ (Merck) and oxalic acid (Aldrich) were used without any further purification. Two methods for the deposition of silver were used: liquid impregnation and photodeposition. The amounts of silver loaded were 0.1, 0.3, 1.0, 2.0 and 5.0 at.%. The metal loading (atomic percentage) was calculated as the ratio between moles of Ag, n_{Ag}, and the totals, n_{Ti} and n_{Ag}, $n_{Ag}/(n_{Ti} + n_{Ag})$. The photocatalysts obtained from impregnation were named xAg-iTiO_2 and those obtained from photodeposition xAg-pTiO_2, where x denominates the silver atomic percentage.

The samples from both methods were then calcined at 400 °C for 2 h. This temperature is high enough to guarantee the elimination of the nitrate from the silver precursor and, at the same time, moderate enough to avoid structural modification of the bare TiO_2.

2.3. Impregnation method

A modification of the impregnation method earlier described by Bickley et al. [23] was applied for the synthesis of Ag loaded TiO_2 photocatalytic materials. 4 g of photocatalyst was added to 1 L of MilliQ water with the appropriate amount of Ag (from $AgNO_3$). This suspension was subjected to vigorous stirring for 1 day on a stirring plate and then evaporated until dry at boiling temperature.

2.4. Photodeposition method

The method employed was a modification of the method described by Iliev et al. [24]. In an immersed reactor with stirring, 2 g of photocatalyst was dispersed into 200 mL of MilliQ water at room temperature. The dissolved oxygen was removed from the solution with nitrogen flow bubbling that was maintained for the whole process. After 30 min, the necessary silver amount was added from 1 M $AgNO_3$ solution. Oxalic acid was added as a sacrificial donor (at a molar ratio oxalic acid:silver = 25:1) and the whole volume was completed with water until 400 mL, resulting in pH <2 in all cases. The suspension was left for a further 30 min in darkness and the slurry was then irradiated with a 400 W medium pressure Hg lamp (8.1×10^{-7} einstein s^{-1} L^{-1}) placed inside a quartz tube, for about 330 min. Continuous stirring and nitrogen sparging was maintained during the whole process. The precipitate was filtered, washed with MilliQ water and then dried at 120 °C for 2 h.

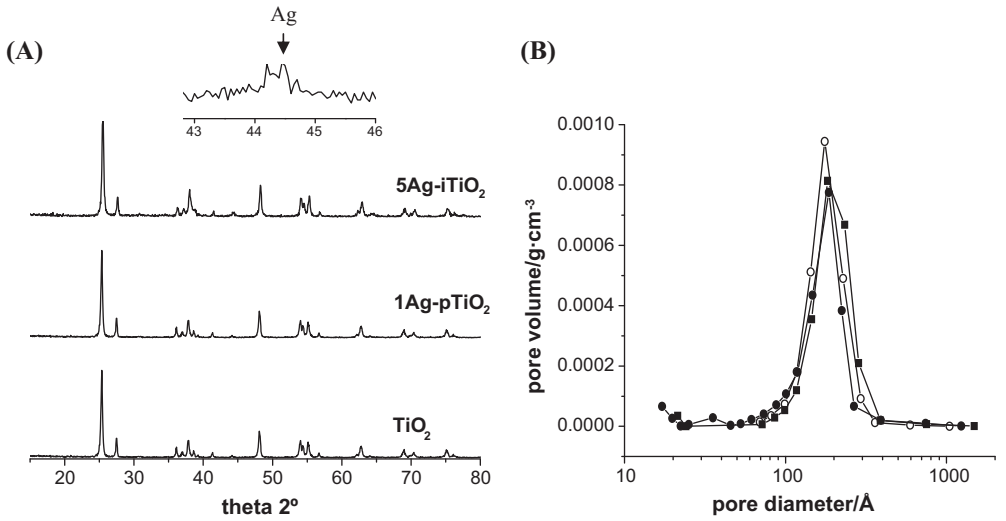

Fig. 1. (A) XRD patterns of bare TiO_2, 1Ag-pTiO_2 and 5Ag-iTiO_2. (B) Pore size distribution of (○) bare TiO_2, (●) 5Ag-iTiO_2 and (■) 1Ag-pTiO_2.

3. Results and discussion

The results corresponding to structural characterization on *x*Ag-TiO_2 are shown in Table 1. It can be observed that the metallized photocatalyst samples show no change, irrespective of the deposition method, either in the crystalline phase ratio or anatase and rutile crystal sizes within the uncertainty of the measurements [19]. Fig. 1(A) shows the diffractograms of the *x*Ag-TiO_2 samples with the highest silver content, 1Ag-pTiO_2 and 5Ag-iTiO_2. It is observed that the presence of neat TiO_2 is barely modified by the presence of silver deposits, and that the various diffraction patterns almost coincide. This suggests that the silver particles are dispersed on the surface and are not covalently bonded in the crystalline structure of TiO_2 [25]. As can be expected in samples with a value of $x = 1$, diffraction peaks of metallic Ag are not observed. However, in the samples with $x = 5$, the diffraction peak at 44.2° (2 0 0) of metallic Ag is observed, denoting its presence on metallized samples. The intensity of the main silver peak at 37.5° can be masked by the TiO_2 layer. Due to the sensitivity of the XRD technique, it was not possible to discern other peaks or silver oxide patterns in photocatalysts with a lower silver amount [26].

However, changes were observed in the surface area value as a result of the incorporation of silver deposits on the TiO_2 surface (see Table 1). The BET specific surface area of the unmodified TiO_2-powder material was previously reported to be 21 $m^2\,g^{-1}$ [21]. The surface area slightly decreases in size as the amount of silver deposition increases, reaching 17 $m^2\,g^{-1}$ for 1Ag-pTiO_2 and 15 $m^2\,g^{-1}$ for 5Ag-iTiO_2 [9,25,27]. This may be because the silver clusters block the TiO_2 capillaries. Fig. 1(B) shows how the pore volume of 5Ag-iTiO_2 and 1Ag-pTiO_2 slightly decrease with respect to the bare TiO_2 volume.

For comparative purposes, the commercial photocatalyst TiO_2 Degussa P25 was subjected to the same silver deposition procedures. It can be seen from Table 2 that the effect of the silver deposits on TiO_2 Degussa P25 was similar to that for the homemade photocatalyst. The diffraction patterns of the samples were not modified by the surface presence of silver, showing similar crystalline phase ratio and crystal sizes to TiO_2 Degussa P25. For both sets of samples, the surface area also decreased in size as the amount of silver deposition rose, from 50 $m^2\,g^{-1}$ to 41 $m^2\,g^{-1}$ for 5Ag-iP25 and to 44 $m^2\,g^{-1}$ for 5Ag-pP25.

Also shown in Tables 1 and 2 are the band gap values. It is observed that for photocatalysts with lower silver deposition the values are similar to those for the bare photocatalysts. However, a fall in the band gap values can be seen for photocatalysts with higher silver deposition, as has been reported by other authors [27,28]. This decrease is because the metallic clusters introduce localized energy levels in the TiO_2 band gap. The electrons can be excited with lower energy from the valence band to these levels rather than to the conduction band of the semiconductor.

Fig. 2(A) shows the diffuse reflectance spectra for *x*Ag-iTiO_2 samples. Beyond the band-gap absorption threshold of titania at $\lambda \leq 380$ nm it is observed that the addition of silver ions and subsequent UV irradiation cause significant changes to the absorption

Table 1
Structural characteristics of photocatalysts *x*Ag-TiO_2.

	S_{BET} ($m^2\,g^{-1}$)	Anatase (nm)	Rutile (nm)	% anatase	Band gap (eV)
TiO_2					
0.0	21 ± 0.321	33	39	78	3.02 ± 0.021
*x*Ag-iTiO_2					
0.1	21 ± 0.121	29	37	82	3.02 ± 0.025
0.3	21 ± 0.221	33	40	81	3.02 ± 0.021
1.0	17 ± 0.117	29	38	82	3.02 ± 0.023
2.0	15 ± 0.115	33	39	82	3.00 ± 0.024
5.0	15 ± 0.115	29	36	80	2.93 ± 0.021
*x*Ag-pTiO_2					
0.1	21 ± 0.121	31	42	78	3.02 ± 0.022
0.3	20 ± 0.119	31	40	78	3.02 ± 0.021
1.0	17 ± 0.117	31	36	77	2.99 ± 0.024

Table 2
Structural characteristics of photocatalysts *x*Ag-P25.

	S_{BET} ($m^2\,g^{-1}$)	Anatase (nm)	Rutile (nm)	% anatase	Band gap (eV)
P25					
0.0	49 ± 0.549	21	28	80	3.09 ± 0.022
*x*Ag-iP25					
0.1	49 ± 0.449	21	29	75	3.08 ± 0.021
0.3	49 ± 0.249	21	29	75	3.08 ± 0.022
1.0	44 ± 0.243	21	29	74	3.05 ± 0.021
2.0	45 ± 0.345	21	32	72	3.01 ± 0.023
5.0	41 ± 0.141	22	32	70	2.94 ± 0.022
*x*Ag-pP25					
0.1	51 ± 0.251	21	36	71	3.08 ± 0.024
0.3	50 ± 0.250	22	29	74	3.08 ± 0.021
1.0	48 ± 0.348	21	32	71	3.07 ± 0.023
2.0	45 ± 0.245	21	30	76	3.03 ± 0.023
5.0	44 ± 0.244	21	33	69	3.03 ± 0.021

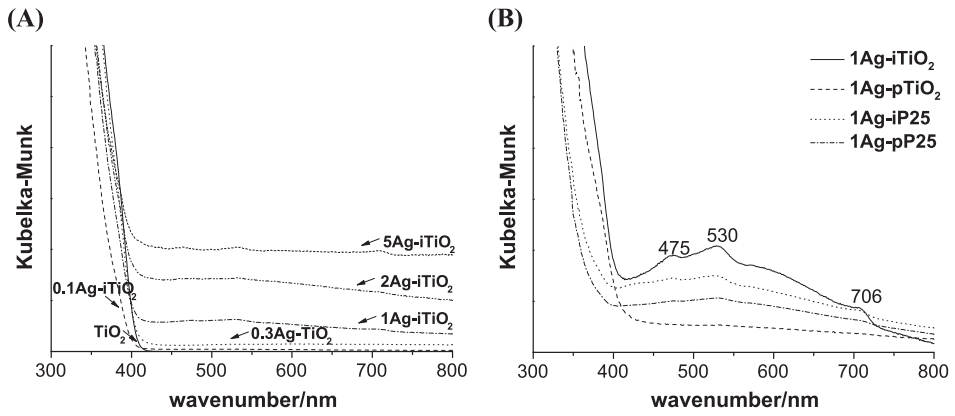

Fig. 2. (A) Diffuse reflectance spectra UV–vis of: bare TiO_2, 0.1Ag-iTiO_2, 0.3Ag-iTiO_2, 1Ag-iTiO_2, 2Ag-iTiO_2 and 5Ag-iTiO_2. (B) Diffuse reflectance spectra UV–vis of: 1Ag-iTiO_2, 1Ag-pTiO_2 and the same corresponding to P25: 1Ag-iP25 and 1Ag-pP25.

spectrum of TiO_2, resulting in high absorbance from 400 nm to the entire visible region [27]. The absorption value is related to the amount of metal deposition, in other words the higher the amount of silver deposition the greater the absorption in the visible region. In addition, absorption is not constant between 420 nm and 800 nm. This underlines the fact that the metallic clusters on the photocatalyst surface are not homogeneous in size. It is known that lack of homogeneity is an inherent feature of wet deposition methods.

The metallic clusters of several metals, such as Au and Ag, lead to the formation of plasmons that have characteristic absorption bands [29–31]. Fig. 2(B) shows the absorption plasmonic bands for 1%Ag samples. The values found in the literature for silver plasmonic bands are very diverse. While Sobana et al. [27] described a band in 440 nm, Rupa et al. [33] reported a wide band centered in 370 nm. In this case a broad band is observed that is the sum of three bands at 475, 530 and 706 nm. It is well known that optical properties of metal nanostructures are strongly related to their shape [32]. However, these values do not coincide with values assigned by Chen et al. [34] for silver nanocubes, silver nanospheres or silver nanoplates. This would seem to suggest a high degree of irregularity in the shapes of the silver deposits obtained in this work. Furthermore, it can be seen from Fig. 2(B) that the plasmons depend on the deposition method employed since the absorption bands are more evident in the samples obtained by impregnation for both homemade TiO_2 and P25, though more Ag^0 and, therefore, absorption would be expected in the samples obtained by photodeposition. This apparent contradiction will be explained in the following sections.

3.1. Morphology study

Figs. 3 and 4 show the SEM and TEM images, respectively, of 1%Ag samples. As we reported in a previous work, bare TiO_2 displays a high degree of size heterogeneity, with spherical particles ranging from 45 nm to as large as 70 nm [21]. Analysis of Figs. 3 and 4 showed that the distribution of silver on the surface of TiO_2 is not uniform. Silver deposits do not totally cover the surface of TiO_2 particles as might occur at larger percentages where the deposit size would be larger [9,35]. It can also be seen from Figs. 3 and 4 that the silver particles are mainly found in the boundaries of TiO_2 particles. The deposits, which are aggregates of tiny crystals, are regular spherical-shaped particles. In concordance with DRS results, there is no homogeneity in the sizes of the deposits resulting from either of the two methods. In terms of size, the impregnation process displays greater heterogeneity. Back-scattered SEM analysis revealed deposits of between 45 and 70 nm, while the TEM analyses revealed smaller deposits of around 10 nm or less. However, photodeposition resulted in larger homogeneity since only deposits lower than 10 nm were found. These differences in deposit size correlate with the fact that absorption plasmonic bands are more evident in the impregnated samples than in the photodeposited ones. In addition, in the *x*Ag-iTiO_2 series a TEM analysis was made of the distribution of silver deposit size. It was observed that as the silver loading increased larger deposit sizes were found (Fig. 4C).

3.2. X-ray dispersive energy (EDX) and X-ray photoelectron spectroscopy (XPS) measurements

Table 3 shows the results of the EDX analyses for the *x*Ag-iTiO_2 series and for the remaining samples with a silver loading of 1% for purposes of comparison. The EDX results for any of the

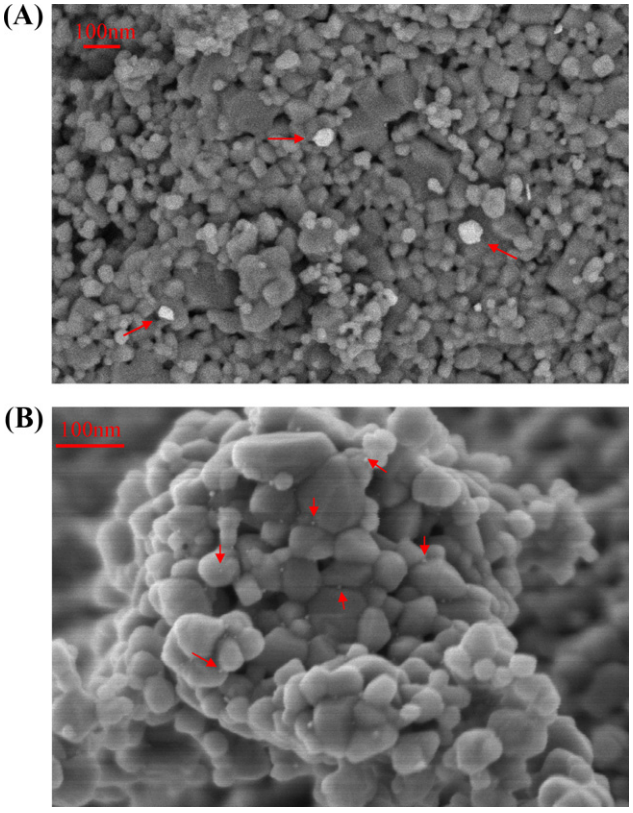

Fig. 3. SEM images of (A) 1Ag-iTiO_2 and (B) 1Ag-pTiO_2.

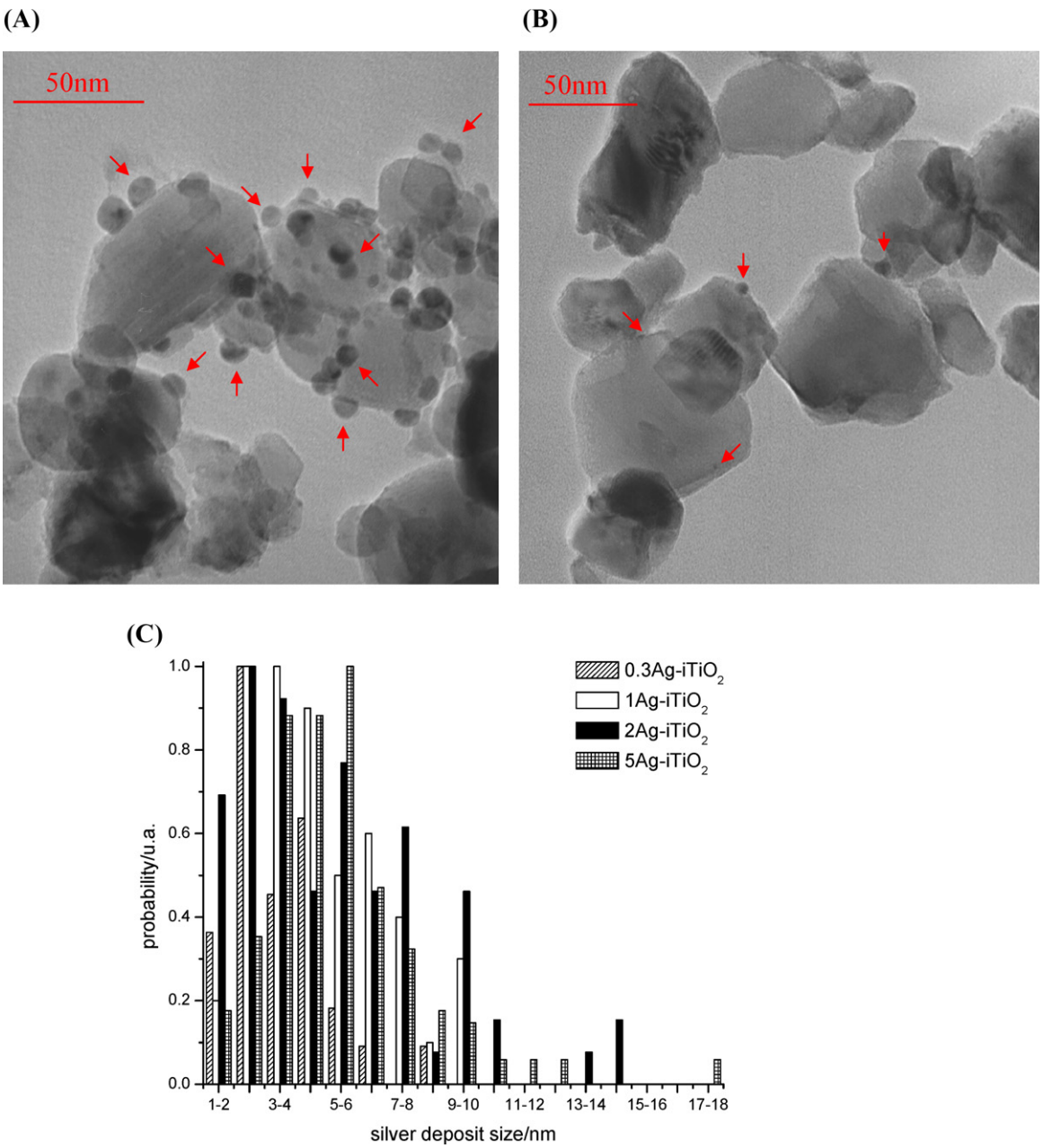

Fig. 4. TEM images of (A) 1Ag-iTiO$_2$, (B) 1Ag-pTiO$_2$ and (C) distribution of the size of silver deposits on *x*Ag-iTiO$_2$ samples.

Table 3
EDX analyses.

	EDX			
	Zone 1		Zone 2	
	Ag (%)	Ti (%)	Ag (%)	Ti (%)
0.1Ag-iTiO$_2$	0.89	99.11	1.39	98.61
0.3Ag-iTiO$_2$	0.49	99.51	0.98	99.02
1Ag-iTiO$_2$	0.71	99.29	3.56	96.44
2Ag-iTiO$_2$	1.53	98.47	3.43	96.57
5Ag-iTiO$_2$	1.88	98.12	6.01	93.99
0.1Ag-pTiO$_2$	0.87	99.13	1.32	98.68
0.3Ag-pTiO$_2$	0.85	99.15	1.12	98.88
1Ag-pTiO$_2$	0.48	99.52	2.87	97.13
1Ag-iP25	1.09	98.91	0.95	99.05
1Ag-pP25	0.92	99.08	1.13	98.87

samples of the *x*Ag-iTiO$_2$ series give very different values for the two zones considered and, in addition, different to the amount of silver quantitatively added in the preparation of the samples. For example, for the samples with 1 at.% Ag, we found values of 0.71 and 3.56 at.% Ag for 1Ag-iTiO$_2$ and 0.48 and 2.87 at.% Ag for 1Ag-pTiO$_2$. This reveals that the deposition of silver on TiO$_2$ was non-uniform as evident in the microscopic images. However, the same analysis performed for TiO$_2$ Degussa P25 revealed greater uniformity in the deposition, with values that approached the theoretical values. This indicates that the deposition is dependent on the bare TiO$_2$ that is being modified [14]. TiO$_2$ Degussa P25 gave rise to a very stable suspension compared to the homemade TiO$_2$ which did not form suspension due to its heavier particles which required continuous stirring to keep them in suspension. As has been reported [21], Degussa P25 exhibits aggregates around 3 μm in aqueous solution compared to around 50 μm for homemade TiO$_2$.

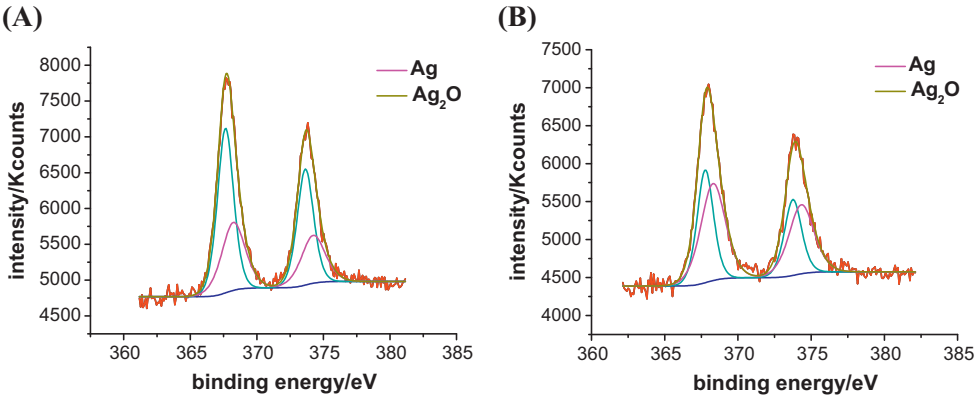

Fig. 5. XPS spectra (Ag $3d_{5/2}$) of: (A) 1Ag-iTiO_2 and (B) 1Ag-pTiO_2. (For interpretation of the references to spectra in this figure legend, the reader is referred to the web version of this article.)

The bonding energy values corresponding to 3d level Ag at different oxidation states (Ag^o, Ag_2O, and AgO) are very similar. Values have been reported for $3d_{5/2}$ of 368.0–368.3 eV, 367.6–367.8 eV, and 367.3–367.4 eV, respectively [35,36]. Since all the values are in a narrow range, it is quite difficult to make a quantitative analysis of the silver chemical species in the deposits on the semiconductor from XPS spectra with any degree of certainty. So, a deconvolution analysis of XPS signals allowed us to qualitatively estimate the presence of Ag^o and Ag_2O in 1Ag-iTiO_2 and 1Ag-pTiO_2 (Fig. 5). A higher ratio of Ag^o/oxidized Ag in the photocatalyst obtained by photodeposition was confirmed by the analysis. Other evidence for this was found in the ratio O(1s)/Ti(2p) (Table 4), which was higher in the impregnated samples, indicating a larger surface quantity of O and, consequently, of oxidized silver.

The XPS results were used to estimate surface dispersion of the deposits. The higher the signal in the XPS spectra, the higher the dispersion in the corresponding metal deposits [37]. It was observed, on this basis, that the Ag-TiO_2 samples obtained by impregnation and photodeposition were very similar in terms of surface dispersion (Table 4).

3.3. Photocatalytic reactivity

The effects of silver metallization of titania on photoactivity were studied by examining the phenol degradation reaction. The reaction rate of photocatalytic degradation of phenol follows a first kinetic order according to the first stage of the Langmuir–Hinshelwood model and its mineralization an apparent zero kinetic order.

Some authors have seen an increase in the adsorption capacity of the photocatalysts by silver surface deposits [33,38,39], while others have described the opposite effect. In the case of the photocatalysts synthesized in this present study, no significant changes in the adsorption capacity were observed. Adsorption of the pollutant was around 2% of the initial concentration. In addition, no phenol was degraded in the absence of illumination, indicating that there was no dark reaction at the Ag-TiO_2 surface.

Table 4
XPS analyses. Binding energy of O(1s) in eV is in brackets in the O:Ti ratio column.

	XPS		
	Ag (%)	Ti (%)	O/Ti
0.3Ag-iTiO_2	0.79	99.21	2.00 (529.8)
1Ag-iTiO_2	3.02	96.98	1.90 (529.7)
5Ag-iTiO_2	10.46	89.54	2.14 (530)
0.3Ag-pTiO_2	0.99	99.01	1.75 (530.0)
1Ag-pTiO_2	2.84	97.16	1.85 (529.9)
1Ag-iP25	2.12	97.88	1.74 (529.8)
1Ag-pP25	2.48	97.52	1.69 (529.8)

Fig. 6 shows the degradation rate constants (k°) and mineralization rate constants (k_{TOC}) for x Ag-iTiO_2 photocatalysts. All the x Ag-iTiO_2 photocatalysts, except the lowest silver loading, 0.1Ag-iTiO_2, degraded phenol faster than bare TiO_2. In the literature, this improvement is attributed mainly to the Ag particles deposited on the TiO_2 acting as electron–hole separation centers [19,40]. Electron transference from the TiO_2 conduction band to silver particles is thermodynamically possible because the Fermi level of TiO_2 is higher than that of silver. This may cause the formation of Schottky barriers at the metal-semiconductor contact region, which improve the charge separation and thus enhance the photocatalytic activity of TiO_2 [27]. The silver deposits act as electron scavengers immobilizing the electrons and transferring them to oxygen to form $O_2^{\bullet-}$ (superoxide radical), which is considered the determining step of the photocatalytic process. The trapping of electrons by the metallic deposits is faster than the transference of electrons to oxygen from bare TiO_2 or its recombination with holes. So, the silver deposits in the surface improve the photoactivity accelerating the transference of trapped electrons in the metallic deposits to the oxygen molecules in solution [19,41].

It was observed that photonic efficiency increased considerably with an increase in the silver loading up to 0.3 at.% and then remained nearly constant for higher silver loading. This degradation plateau indicates that the effective quantity of holes and electrons that a deposit of 0.3% silver facilitates is sufficient for the degradation of an initial concentration of 50 ppm of phenol and any increase in the silver loading will mean that there is an excess concentration of oxidizing agents (holes or hydroxyl radicals) with respect to the concentration of phenol. There is no improvement in the reaction rate and if the desire is to use the higher number of holes available for oxidation on the photocatalysts with more than 0.3 at.% Ag then a higher number of molecules of the pollutant to be photodegraded will be required. A similar case was observed by Vamathevan et al. for sucrose [42].

With respect to mineralization (Fig. 6B), the behavior is very different. The mineralization rate increased for silver content from 0.1% to 0.3%, rising above the rate for bare TiO_2. However, when silver content was higher than 0.3% the mineralization rate fell to values lower than for bare TiO_2. It seems that the highest silver percentages are detrimental to the degradation of phenol by-products illustrating that the role of silver-modified TiO_2 particles is dependent on the type of organic compound involved. Finally, based on the degradation and mineralization results, silver content of 0.3% was the optimum loading.

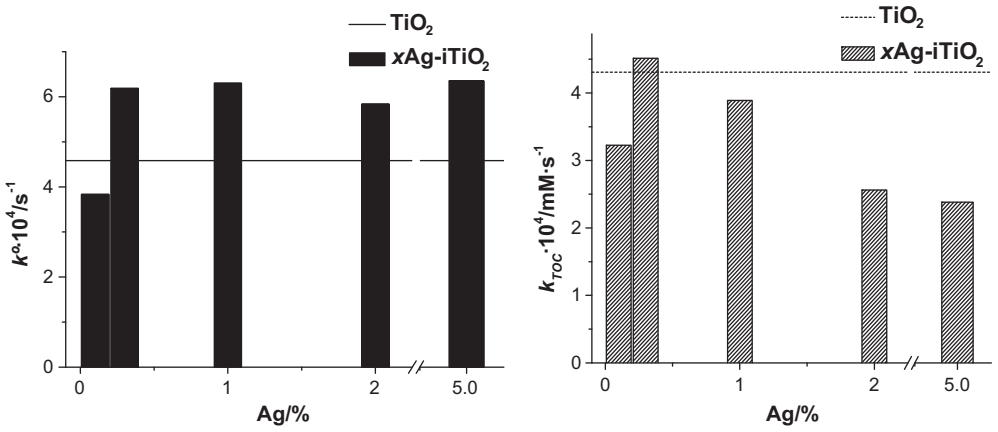

Fig. 6. Degradation rate constants (k°) and mineralization rate constants (k_{TOC}) for xAg-iTiO$_2$: C_o (phenol) 50 ppm, pH$_o$ 5, 1 g L^{-1} photocatalyst.

A comparison was also undertaken of the photoactivity of the samples obtained by photodeposition and impregnation. An analysis of the results shown in Table 5 revealed that the samples obtained by impregnation showed slightly higher kinetic constant values in both degradation and mineralization. These differences could be due to the smaller size of the silver deposits found in xAg-pTiO$_2$ than in xAg-iTiO$_2$, which trap the holes faster and favor recombination. However, some authors justify the differences in photoactivity on the basis of the silver oxidation state on the semiconductor surface after the deposition process [36]. As stated in Section 3.2, there is a larger amount of metallic silver in the photocatalysts obtained by photodeposition than in those obtained by impregnation where there is predominantly oxidized silver. So, the xAg-iTiO$_2$ photocatalysts have a greater capacity to reduce the electron/hole recombination as a result of the silver ions consuming electrons which gives rise to metallic silver [42].

To determine the effect of the 0.3Ag-iTiO$_2$ load, a set of experiments was carried out varying the amount of photocatalyst from 1 to 4 g L^{-1}. The kinetic constants for various photocatalyst loads are depicted in Fig. 7. It can be seen how the kinetic constant exhibits a sharp increase raising the photocatalyst concentration to 3 g L^{-1}, while above this concentration it decreases. This pattern (although with an optimum load at 2 g L^{-1}) has been reported for bare TiO$_2$ in another study [21]. This increase in degradation up to a photocatalyst load of 3 g L^{-1} is due to the rise in available active and adsorption sites. However, when the photocatalyst load rises above the optimum value, the rates decrease as the suspended particles of the photocatalyst block the UV-light passage and the light scattering increases [43]. Although the optimum load for the 0.3Ag-iTiO$_2$ photocatalyst is higher than for unmodified TiO$_2$, 3 g L^{-1} *vs.* 2 g L^{-1}, the degradation rate constant increases considerably (12.52 *vs.* 7.43 s^{-1}).

The literature shows how modification of the photocatalyst surface by metallic deposition does not always improve photoactivity, sometimes having the opposite or no effect [38]. In this respect, the properties of the semiconductor surface to be modified are the

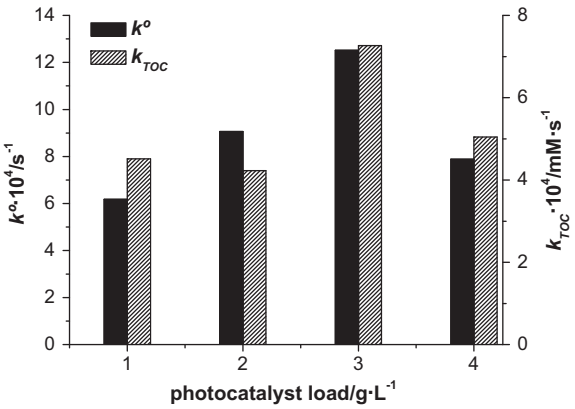

Fig. 7. Degradation rate constants (k°) and mineralization rate constants (k_{TOC}) for xAg-iTiO$_2$ depending on the photocatalyst load: C_o (phenol) 50 ppm, pH$_o$ 5.

determining factor. In Fig. 8, it is observed that the modification here shown for TiO$_2$ Degussa P25 by silver impregnation resulted in a fall in photoactivity for phenol. This indicates that the presence of silver acting as an electron scavenger may have little effect on charge separation efficiency which is overwhelmingly due to the photocatalyst structure, the crystalline phases and how they are connected. Surface modification by silver deposition inhibits the activity, possibly as a result of blockage of active centers.

Table 5
Degradation rate constants (k°) and mineralization rate constants (k_{TOC}) for xAg-iTiO$_2$ and xAg-pTiO$_2$: C_o (phenol) 50 ppm, pH$_o$ 5, 1 g L^{-1} photocatalyst.

%Ag	xAg-iTiO$_2$		xAg-pTiO$_2$	
	$k^{\circ} \times 10^4$ (s^{-1})	$k_{TOC} \times 10^4$ (mM s^{-1})	$k^{\circ} \times 10^4$ (s^{-1})	$k_{TOC} \times 10^4$ (mM s^{-1})
0.1	3.83	3.23	3.45	2.03
0.3	6.18	4.52	5.46	3.90
1.0	6.30	3.89	4.53	3.55

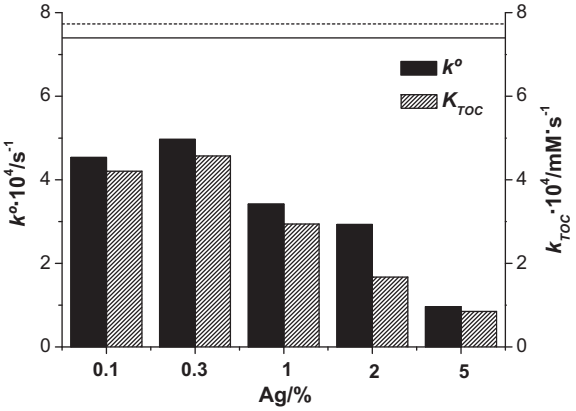

Fig. 8. Degradation rate constants (k°) and mineralization rate constants (k_{TOC}) for xAg-iP25 where lines correspond to TiO$_2$ Degussa P25 (1 g L^{-1} photocatalyst, C_o (phenol) 50 ppm, pH$_o$ 5).

Table 6
Degradation rate constants ($k^{\circ} \times 10^4$, s^{-1}) of phenol, phthalic acid, *2,4*-dichlorophenol and *m*-cresol for the optimum photocatalyst load of Degussa P25, homemade TiO_2 and 0.3Ag-iTiO_2.

Pollutant	Degussa P25	Homemade TiO_2	0.3Ag-iTiO_2
Phenol	7.82	7.05	12.52
Phthalic acid	4.45	9.58	9.35
2,4-Dichlorophenol	6.15	7.35	13.40
m-Cresol	5.47	5.78	8.65

As the activity of silver/titania particles is dependent on the nature of the organic compound to photo-oxidase [44], the effectiveness of 0.3Ag-iTiO_2 was tested for other pollutants such as *2,4*-dichlorophenol, phthalic acid and *m*-cresol, giving better results than those obtained with non-modified TiO_2 and Degussa P25 TiO_2 (Table 6).

3.4. Reutilization studies

The reuse capacity of 0.3Ag-iTiO_2 was tested. Importantly, silver-deposited TiO_2 nanoparticles were readily separated from the suspension by settling alone and no coagulant needed to be added to the system as reported for bare TiO_2 [21]. As shown in Fig. 9, efficiency fell only slightly. While after the first use only 2% of initial phenol in solution remained after 90 min degradation, in the second use this percentage rose to 6% and to 10% in the fourth use. This efficiency decrease is due to two factors: firstly, to the relative increase in reduced silver in the surface deposits at the beginning of the following use due to its reduction during the photocatalytic test [10] and, secondly, to leaching of the deposits. Both factors can be seen in the atomic absorption measurements (Fig. 9). Just before lighting, after a period of 30 min in darkness to reach the adsorption equilibrium, Ag leaching can be observed. The quantity of Ag^+ ions dissolved from 0.3Ag-iTiO_2 was 1.27 ppm. Once illumination commenced, the silver quickly returned to the photocatalyst by photo-reduction leaving around 20 ppb that remained in the photocatalyst bulk until the end of the photocatalytic run. Similar concentration profiles of silver were also observed in all the reuse tests. These results are consistent with the important role that oxidized silver plays in improving the photocatalytic activities of *x*Ag-TiO_2 photocatalysts and underlines the need to find a simple and practical method for Ag^+ recycling before each photocatalytic run.

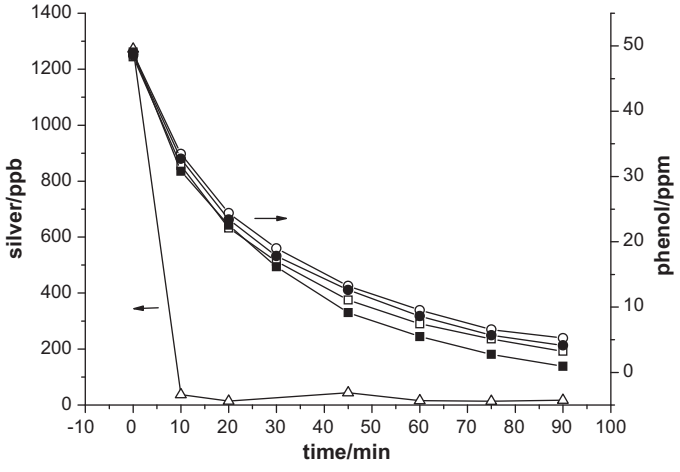

Fig. 9. Phenol concentration profile for 1 g L^{-1} 0.3Ag-iTiO_2 (C_o 50 ppm, pH_o 5): (■) 1st use, (□) 2nd use, (●) 3rd use, (○) 4th use and $[Ag]_{aq}$ during phenol degradation in the 1st use of the photocatalyst.

Conclusions

Silver in low amounts may play a favorable role in the enhancement of photocatalytic activity by attracting electrons, thus helping electron–hole pair separation and preventing electron–hole recombination. Due to the higher Ag^+/Ag ratio, better results were obtained with the impregnation method than the photodeposition method. This is because the enhancement of UV photocatalytic activity of *x*Ag-TiO_2 photocatalysts is based on the improvement of quantum efficiency caused by a sacrifice of oxidized silver. Optimum metal loading was 0.3 at.% Ag and the photocatalyst 0.3Ag-iTiO_2, which is easily obtained, showed greater efficiency than bare TiO_2 and P25 for different pollutants. Its easy recovery creates advantageous conditions for repeat use with low losses in efficiency. Consequently, from a practical application point of view, it is highly advantageous to add silver to titania photocatalysts.

Acknowledgements

We are grateful for the funding of the European Commission through the Clean Water Project which is a Collaborative Project (Grant Agreement number 227017) co-funded by the Research DG of the European Commission within the joint RTD activities of the Environment and NMP Thematic Priorities. We would also like to thank the Spanish Ministry of Science and Innovation for their financial support through the Project CTQ2008-05961-C02-02, CTQ2008-05961-C02-01. Finally, E. Pulido Melián expresses her gratitude for the support of the FPI Grant Program of the Spanish Ministry of Education and Science.

References

[1] I. Poulios, E. Micropoulou, R. Panou, E. Kostopoulou, Applied Catalysis B: Environmental 41 (2003) 345–355.
[2] A.J. Maira, W.N. Lau, C.Y. Lee, P.L. Yue, C.K. Chan, K.L. Yeung, Chemical Engineering Science 58 (2003) 959–962.
[3] A. Kubacka, M. Fernández-García, G. Colón, Chemical Reviews 112 (2012) 1555–1614.
[4] M. Maicu, M.C. Hidalgo, G. Colón, J.A. Navío, Journal of Photochemistry and Photobiology A: Chemistry 217 (2011) 275–283.
[5] M.C. Hidalgo, J.J. Murcia, J.A. Navío, G. Colón, Applied Catalysis A: Chemical 397 (2011) 112–120.
[6] H.M. Sung-Suh, J.R. Choi, H.J. Hah, S.M. Koo, Y.C. Bae, Journal of Photochemistry and Photobiology A: Chemistry 163 (2004) 37–44.
[7] M.A. Rauf, M.A. Meetani, S. Hisaindee, Desalination 276 (2011) 13–27.
[8] N. Sobana, K. Selvam, M. Swaminathan, Separation and Purification Technology 62 (2008) 648–653.
[9] H. Li, X. Duan, G. Liu, X. Liu, Journal of Materials Science 43 (2008) 1669–1676.
[10] W. Zhou, H. Liu, J. Wang, D. Liu, G. Du, J. Cui, Applied Materials and Interfaces 8 (2010) 2385–2392.
[11] A. Sclafani, J.M. Herrmann, Journal of Photochemistry and Photobiology 113 (1998) 181–188.
[12] O. Carp, C.L. Huisman, A. Reller, Progress in Solid State Chemistry 32 (2004) 133–177.
[13] H.M. Coleman, K. Chiang, R. Amal, Journal of Chemical Engineering 113 (2005) 65–72.
[14] R. Tongpool, K. Setwong, C. Mai, Journal of Science 35 (2008) 274–282.
[15] J. Ryu, W. Choi, Environmental Science and Technology 42 (2007) 294–300.
[16] M.M. Kondo, W.F. Jardim, Water Research 25 (1991) 823–827.
[17] C. Sahoo, A.K. Gupta, A. Pal, Dyes Pigments 66 (2005) 189–196.
[18] A. Ozkan, M.H. Ozkan, R. Gurkan, M. Akay, M. Sokmen, Journal of Photochemistry and Photobiology A 163 (2004) 29–35.
[19] M.A. Behnajady, N. Modirshahla, M. Shokri, B. Rad, Global Nest Journal 10 (2008) 1–7.
[20] A. Orlov, D.A. Jefferson, N. Macleod, R.M. Lambert, Catalysis Letters 92 (2004) 41–47.
[21] E. Pulido Melián, O. González Díaz, J.M. Doña Rodríguez, G. Colón, J.A. Navío, J. Pérez Peña, Applied Catalysis A: General 411–412 (2012) 153–159.
[22] S.P. Tandon, J.P. Gupta, Physica Status Solidi 38 (1970) 363–367.
[23] R.I. Bickley, J.S. Lees, R.J.D. Tilley, L. Palmisano, M. Schiavello, Journal of the Chemical Society, Faraday Transactions 88 (1992) 377–383.
[24] V. Iliev, D. Tomova, L. Bilyarska, A. Eliyas, L. Petrov, Applied Catalysis B: Environmental 63 (2006) 266–271.
[25] S. Sakthivel, M.V. Shankar, M. Palanichamy, B. Arabindoo, D.W. Bahnemann, V. Murugesan, Water Research 38 (2004) 3001–3008.

[26] M. Jin, X. Zhang, S. Nishimioto, Z. Liu, D.A. Tryk, A.V. Emeline, T. Murakami, A. Fujishima, Journal of Physical Chemistry C 111 (2007) 658–665.
[27] N. Sobana, M. Muruganadham, M. Swaminathan, Journal of Molecular Catalysis A: Chemical 258 (2006) 124–132.
[28] A.A. Ashkarran, Journal of Theoretical and Applied Physics 4 (4) (2011) 1–8.
[29] K. Awazu, M. Fujimaki, C. Rockstuhl, J. Tominaga, H. Murakami, Y. Ohki, N. Yoshida, T. Watanabe, Journal of the American Chemical Society 130 (2008) 1676–1680.
[30] W. Hou, Z. Liu, P. Pavaskar, W.H. Hung, S.B. Cronin, Journal of Catalysis 277 (2011) 149–153.
[31] S. Linic, P. Christopher, D.B. Ingram, Nature Materials 10 (2011) 911–921.
[32] M. Westphalen, U. Kreibig, J. Rostalski, H. Luth, D. Meissner, Solar Energy Materials and Solar Cells 61 (2000) 97–105.
[33] A.V. Rupa, D. Manikandan, D. Divakar, T. Sivakumar, Journal of Hazardous Materials 147 (2007) 906–913.
[34] E. Chen, H. Su, W. Zhang, T. Tan, Powder Technology 212 (2011) 166–172.
[35] X. You, F. Chen, J. Zhang, M. Anpo, Catalysis Letters 102 (2005) 247–250.
[36] H. Xinggang, W. Xiaoling, L. Andong, Frontiers of Chemistry in China 4 (2006) 402–407.
[37] G. Colón, M. Maicu, M.C. Hidalgo, J.A. Navío, A. Kubacka, M. Fernández-García, Journal of Molecular Catalysis A: Chemical 320 (2010) 14–18.
[38] B. Tryba, M. Piszcz, A.W. Morawski, Open Materials Science Journal 4 (2010) 5–8.
[39] L. Ren, Y.P. Zeng, D. Jiang, Catalysis Communications 10 (2009) 645–649.
[40] J.M. Herrmann, in: R.T.K. Baker, S.J. Tauster, J.A. Dumesic (Eds.), Strong Metal–Support Interactions, vol. 298, ACS Symposium Series, 1986, p. 200.
[41] E. Szabó-Bárdos, H. Czili, A. Horváth, Journal of Photochemistry and Photobiology A 154 (2003) 195–201.
[42] V. Vamathevan, R. Amal, D. Beydoun, G. Low, S. McEvoy, Journal of Photochemistry and Photobiology A 148 (2002) 233–245.
[43] N. Daneshvar, D. Salari, A.R. Khataee, Journal of Photochemistry and Photobiology A: Chemistry 162 (2004) 317–322.
[44] R. Ryu, W. Choi, Environmental Science and Technology 42 (2008) 294–300.